REPORT DOCUMENTATION PAGE

Form Approved OMB NO. 0704-0188

The public reporting burden for this collection of information is estimated to average 1 hour per response, including the time for reviewing instructions, searching existing data sources, gathering and maintaining the data needed, and completing and reviewing the collection of information. Send comments regarding this burden estimate or any other aspect of this collection of information, including suggesstions for reducing this burden, to Washington Headquarters Services, Directorate for Information Operations and Reports, 1215 Jefferson Davis Highway, Suite 1204, Arlington VA, 22202-4302. Respondents should be aware that notwithstanding any other provision of law, no person shall be subject to any oenalty for failing to comply with a collection of information if it does not display a currently valid OMB control number.
PLEASE DO NOT RETURN YOUR FORM TO THE ABOVE ADDRESS.

1. REPORT DATE (DD-MM-YYYY)	2. REPORT TYPE	3. DATES COVERED (From - To)
10-08-2023	Final Report	11-Jul-2019 - 10-Apr-2023

4. TITLE AND SUBTITLE
Final Report: Interfacial Misfit Dislocation Array based Metamorphic Antimonide Buffers for LWIR Detectors

5a. CONTRACT NUMBER
W911NF-19-1-0370

5b. GRANT NUMBER

5c. PROGRAM ELEMENT NUMBER
611102

6. AUTHORS

5d. PROJECT NUMBER

5e. TASK NUMBER

5f. WORK UNIT NUMBER

7. PERFORMING ORGANIZATION NAMES AND ADDRESSES
University of New Mexico Albuquerque
1700 Lomas Boulevard NE, Suite 2200, MSC01 1247
1 University of New Mexico
Albuquerque, NM 87131 -0001

8. PERFORMING ORGANIZATION REPORT NUMBER

9. SPONSORING/MONITORING AGENCY NAME(S) AND ADDRESS (ES)
U.S. Army Research Office
P.O. Box 12211
Research Triangle Park, NC 27709-2211

10. SPONSOR/MONITOR'S ACRONYM(S)
ARO

11. SPONSOR/MONITOR'S REPORT NUMBER(S)
75471-PE.10

12. DISTRIBUTION AVAILIBILITY STATEMENT
Approved for public release; distribution is unlimited.

13. SUPPLEMENTARY NOTES
The views, opinions and/or findings contained in this report are those of the author(s) and should not contrued as an official Department of the Army position, policy or decision, unless so designated by other documentation.

14. ABSTRACT

15. SUBJECT TERMS

16. SECURITY CLASSIFICATION OF:			17. LIMITATION OF ABSTRACT	15. NUMBER OF PAGES	19a. NAME OF RESPONSIBLE PERSON
a. REPORT	b. ABSTRACT	c. THIS PAGE			Ganesh Balakrishnan
UU	UU	UU	UU		19b. TELEPHONE NUMBER 505-259-6412

Standard Form 298 (Rev 8/98)
Prescribed by ANSI Std. Z39.18

RPPR Final Report
as of 14-Aug-2023

Agency Code: 21XD

Proposal Number: 75471PE
Agreement Number: W911NF-19-1-0370

INVESTIGATOR(S):

Name: Ganesh Balakrishnan
Email: gunny@unm.edu
Phone Number: 5052596412
Principal: Y

Organization: **University of New Mexico Albuquerque**
Address: 1700 Lomas Boulevard NE, Suite 2200, MSC01 1247, Albuquerque, NM 871310001
Country: USA
DUNS Number: 868853094
EIN: 856000642

Report Date: 10-Oct-2022
Date Received: 10-Aug-2023
Final Report for Period Beginning 11-Jul-2019 and Ending 10-Apr-2023
Title: Interfacial Misfit Dislocation Array based Metamorphic Antimonide Buffers for LWIR Detectors
Begin Performance Period: 11-Jul-2019
End Performance Period: 10-Apr-2023
Report Term: 0-Other

Submitted By: Ganesh Balakrishnan
Email: gunny@unm.edu
Phone: (505) 259-6412

Distribution Statement: 1-Approved for public release; distribution is unlimited.

STEM Degrees: 3
STEM Participants: 5

Major Goals: The following are the major goals of the proposal:

1) Goal 1: development of ternary antimonide buffers with ~ 6.3 A lattice constant through novel interfacial misfit dislocation arrays. This would involve growth of InGaAs on InP and then subsequent growth of an InGaSb IMF layer. This goal will also involve significant characterization of the materials growth using TEM and XRD to determine residual threading dislocation density.

2) Goal 2: investigation of atomic structure of IMF lower dislocations using transmission electron microscopy.

2) Goal 3: development of the IMF based buffers on Silicon substrates. This will involve both the suppression of antiphase domains and the reduction of threading dislocations. Demonstration of devices based on this approach.

Accomplishments: Key accomplishments:

1) first demonstration of IMF array formation in InSb on InAs and InGaSb on InP.

2) Most significant and complete analysis of IMF arrays using TEM analysis.

3) Demonstration of an ICLED on Silicon in collaboration with NRL.

See upload section for detailed information on accomplishments along with experimental data.

Training Opportunities: Multiple graduate students were trained on the growth of semiconductors using Molecular Beam Epitaxy. Students were also trained on the use transmission electron microscopy. Students were given access to the CINT facility at Sandia National Laboratory and Kevin Reilly upon graduating with a PhD has been offered a Postdoc position at SNL.

Results Dissemination: Students funded on this grant presented in numerous conferences. These include the EMC (2021, 2022, 2023), NAMBE (2022), and CSW (2022).

Two publications were published with two more manuscripts under preparation.

Honors and Awards: Kevin Reilly was awarded the DEPS student fellowship. He also graduated with distinction.

Protocol Activity Status:

Technology Transfer: Nothing to Report

PARTICIPANTS:

Participant Type: PD/PI
Participant: ganesh balakrishnan
Person Months Worked: 1.00 **Funding Support:**
Project Contribution:
National Academy Member: N

Participant Type: Faculty
Participant: Thomas Rotter
Person Months Worked: 3.00 **Funding Support:**
Project Contribution:
National Academy Member: N

Participant Type: Graduate Student (research assistant)
Participant: Kevin Reilly
Person Months Worked: 12.00 **Funding Support:**
Project Contribution:
National Academy Member: N

Participant Type: Graduate Student (research assistant)
Participant: Alex Newell
Person Months Worked: 6.00 **Funding Support:**
Project Contribution:
National Academy Member: N

Participant Type: Undergraduate Student
Participant: Carter Heinrich
Person Months Worked: 12.00 **Funding Support:**
Project Contribution:
National Academy Member: N

Participant Type: Graduate Student (research assistant)
Participant: Mega Frost
Person Months Worked: 3.00 **Funding Support:**
Project Contribution:
National Academy Member: N

RPPR Final Report
as of 14-Aug-2023

ARTICLES:

Publication Type: Journal Article Peer Reviewed: Y **Publication Status:** 1-Published
Journal: Journal of Vacuum Science & Technology A
Publication Identifier Type: DOI Publication Identifier: 10.1116/6.0002681
Volume: 41 Issue: 5 First Page #:
Date Submitted: 8/9/23 12:00AM Date Published: 9/1/23 6:00AM
Publication Location:
Article Title: MBE growth of In0.53Ga0.47Sb on In0.53Ga0.47As/InP substrates using the interfacial misfit dislocation arrays
Authors: Fatih F. Ince, Mega Frost, Subhashree Seth, Darryl Shima, Thomas J. Rotter, Ganesh Balakrishnan
Keywords: Semiconductors, Crystallographic defects, Crystal lattices, Crystal orientation, Optical microscopy, Thermal effects, Transmission electron microscopy, High resolution X-ray diffraction
Abstract: We present the growth of highly relaxed In0.53Ga0.47Sb buffers on In0.53Ga0.47As/InP by inducing a periodic array of interfacial misfit dislocation arrays at the In0.53Ga0.47Sb/ In0.53Ga0.47As interface. The periodic 90° misfit dislocation array is realized through As for Sb anion exchange while keeping the group III sublattice the same. Transmission electron microscopy (TEM) results show the presence of misfit dislocations with a periodicity of 6.16?nm, which corresponds to 14 In0.53Ga0.47Sb lattice sites or 15 In0.53Ga0.47As lattice sites. The In0.53Ga0.47Sb epilayer, however, is affected by phase segregation as evidenced by both TEM and Nomarski optical phase microscopy. The x ray based reciprocal space mapping indicates relaxation to be 99.5% for the In0.53Ga0.47Sb epilayer.
Distribution Statement: 1-Approved for public release; distribution is unlimited.
Acknowledged Federal Support: **Y**

Publication Type: Journal Article Peer Reviewed: Y **Publication Status:** 1-Published
Journal: Journal of Applied Physics
Publication Identifier Type: DOI Publication Identifier: 10.1063/5.0027044
Volume: 128 Issue: 22 First Page #:
Date Submitted: 8/9/23 12:00AM Date Published: 12/1/20 7:00AM
Publication Location:
Article Title: A transmission electron microscopy study of dislocation propagation and filtering in highly mismatched GaSb/GaAs heteroepitaxy
Authors: S. J. Addamane, D. M. Shima, A. Mansoori, G. Balakrishnan
Keywords: transmission electron microscopy, dislocation network, misfit dislocations, threading dislocations, GaSb, GaAs
Abstract: We present the growth of highly relaxed In0.53Ga0.47Sb buffers on In0.53Ga0.47As/InP by inducing a periodic array of interfacial misfit dislocation arrays at the In0.53Ga0.47Sb/ In0.53Ga0.47As interface. The periodic 90° misfit dislocation array is realized through As for Sb anion exchange while keeping the group III sublattice the same. Transmission electron microscopy (TEM) results show the presence of misfit dislocations with a periodicity of 6.16?nm, which corresponds to 14 In0.53Ga0.47Sb lattice sites or 15 In0.53Ga0.47As lattice sites. The In0.53Ga0.47Sb epilayer, however, is affected by phase segregation as evidenced by both TEM and Nomarski optical phase microscopy. The x ray based reciprocal space mapping indicates relaxation to be 99.5% for the In0.53Ga0.47Sb epilayer.
Distribution Statement: 1-Approved for public release; distribution is unlimited.
Acknowledged Federal Support: **Y**

CONFERENCE PAPERS:

Publication Type: Conference Paper or Presentation **Publication Status:** 1-Published
Conference Name: Compound Semiconductor Week 2022 (CSW 2022)
Date Received: 09-Aug-2023 Conference Date: 01-Jun-2022 Date Published: 01-Aug-2022
Conference Location: University of Michigan
Paper Title: Techniques for reduction of threading dislocations in metamorphic growth of GaSb on GaAs for realization of high mobility n and p channels.
Authors: Fatih Ince (Contributed), Alex Newell, Kevin Reilly, Subhashree Seth, Thomas Rotter, Ahmad Mansoori,
Acknowledged Federal Support: **Y**

Publication Type: Conference Paper or Presentation **Publication Status:** 1-Published
Conference Name: CSW 2022
Date Received: 09-Aug-2023 Conference Date: 01-Jun-2022 Date Published: 01-Jun-2022
Conference Location: University of Michigan
Paper Title: Growth of high Indium Percentage InGaSb on InP substrates using the interfacial misfit dislocation array growth mode
Authors: Fatih Ince (Contributed), Alex Newell, Kevin Reilly, Subhashree Seth, Thomas Rotter, Ahmad Mansoori
Acknowledged Federal Support: **Y**

Publication Type: Conference Paper or Presentation **Publication Status:** 1-Published
Conference Name: 2022 IEEE Research and Applications of Photonics in Defense Conference (RAPID)
Date Received: 09-Aug-2023 Conference Date: 12-Sep-2022 Date Published:
Conference Location: Miramar Beach, FL, USA
Paper Title: Interband Cascade LEDs Grown on Silicon
Authors: C. L. Canedy, W. W. Bewley, S. Tomasulo, C. S. Kim, M. Kim, C. D. Merritt, I. Vurgaftman, J. R. Meyer,
Acknowledged Federal Support: **Y**

Partners

,

I certify that the information in the report is complete and accurate:
Signature: Ganesh Balakrishnan
Signature Date: 8/10/23 1:45PM

Final Report for

Contract Number: W911NF1910370
Dates Covered: Jul, 11 2019 to Apr, 10 2023

Organization
The University of New Mexico
Albuquerque, 871310001, USA

Investigators:
Dr. Balakrishnan, Ganesh
Email: gunny@unm.edu
Phone Number: 5052596412

Goal 1: Growth of high Indium Percentage In(Ga)Sb on InP and InAs substrates using the interfacial misfit dislocation array growth mode.

Key results:

1) First demonstration of high quality InSb buffers on InAs with epitaxial quality rivalling GaSb on GaAs.
2) First demonstration of IMF formation in growth of $In_{0.53}Ga_{0.47}Sb$ on InP. There are still some miscibility gap issues that need to rectify.

1.A. MBE growth of IMF InSb on InAs.

To cover the MWIR spectrum and reach the long wave infrared region (LWIR), type II superlattices such as InAs/InAsSb and bulk InAsSb using metamorphic buffers are being developed. Even though using metamorphic buffers can cover a certain range of the spectrum by adjusting arsenic to antimony content of $InAs_xSb_{1-x}$, it is a challenging task considering the repeatability and very thick buffer layers (4µm). In the past, it has been shown that a direct growth of GaSb on GaAs is possible with threading dislocation density being 10^8's per cm^3 and further reduction is possible with the use of defect filter layers. In this grant, we have utilized interfacial misfit dislocations to grow fully relaxed InSb on InAs substrate as well as direct growth of $Al_xIn_{1-x}Sb$ buffer layers on InAs, similar to the GaSb/GaAs system. Developing a fully relaxed, low dislocation density buffer layer will be the basis for developing tunable InAsSb absorber for MWIR and LWIR applications. In figure 1 we see two approaches to the growth of InSb on InAs. The first one is just a binary-to-binary transition and the second involves the growth of an AlInSb layer such that quantum confined structures can be realized.

- Interfacial Misfit Arrays are typically formed by Group V exchange.
- This method is effectively shown in **GaSb/GaAs** system

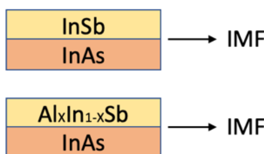

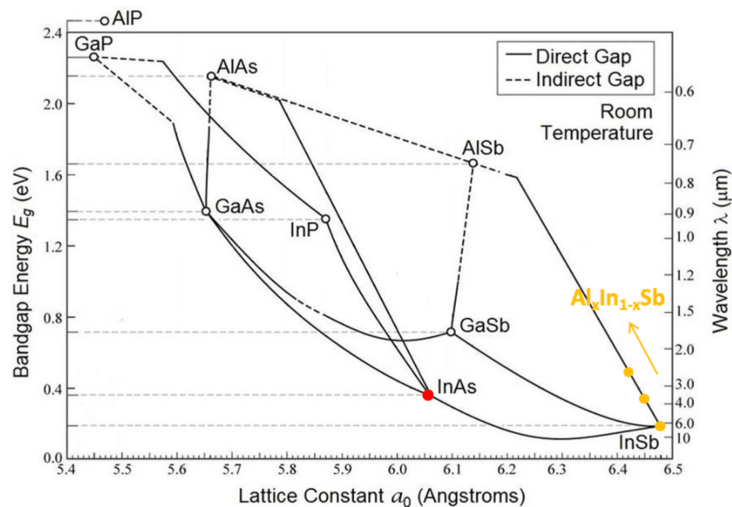

Fig. 1. Growth of InSb and AlInSb IMF layers on InAs substrates.

The MBE growth of InSb growth on InAs process starts with the oxide removal at 530 ^{0}C for 20 minutes and 100 nm of InAs smoothing layer is grown. To grow fully relaxed InSb using interfacial misfit dislocation arrays, excess arsenic must be replaced with antimony to prepare the surface for growth. So, the arsenic supply is cut off and reflection high energy electron diffraction (RHEED) system is used to observe the process. The RHEED pattern turns to 4x from 2x in the

absence of arsenic supply which indicates the transition of group V rich to group III rich surface. Experiments shows that this time varies from 3 to 6 minutes depending on the sample. Since the variation of the transition of group V to group III rich. Thus, the process was controlled manually by looking at the RHEED pattern transition, and extra 30 seconds were added after the transition to allow uniformity along the substrate. This process is followed up by growing 500 nm thick $Al_{0.2}In_{0.8}Sb$ and $Al_{0.1}In_{0.9}Sb$ buffer layers to optimize the buffer layers with different growth temperatures. Finally, InSb quantum well samples were grown with varied Al content AlInSb buffer layers for the analysis.

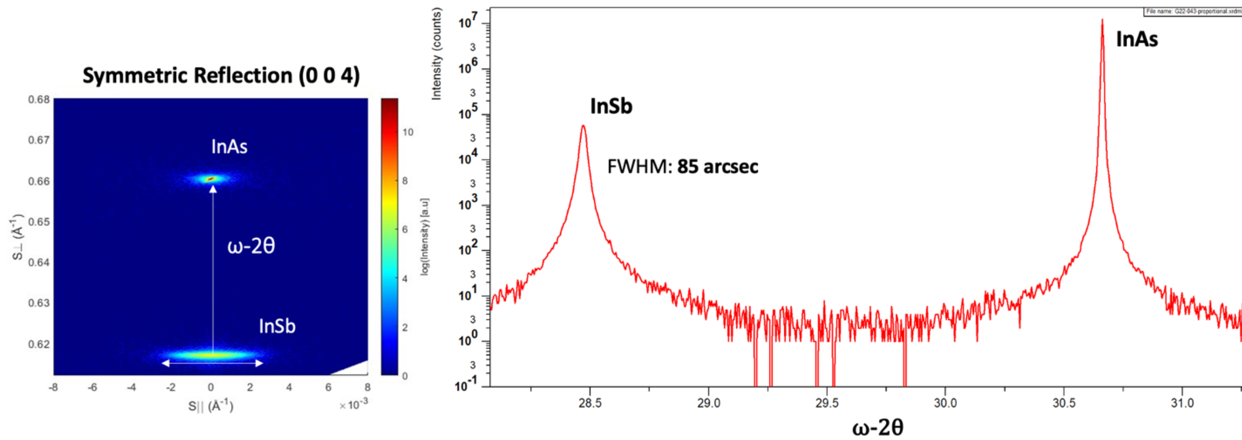

Fig. 2. High quality InSb realized on InAs with 85 arcsec FWHM.

Both the direct grown AlInSb and InSb epilayers on InAs substrate are analyzed using HR-XRD of ω-2θ scans as well as reciprocal space mapping to quantify the dislocation density of the buffer layers. HR-XRD indicates the relaxation of 99.4% for the direct growth of InSb on InAs. By using reciprocal space mapping, screw and mixed dislocation density is found to be $10^8/cm^2$.

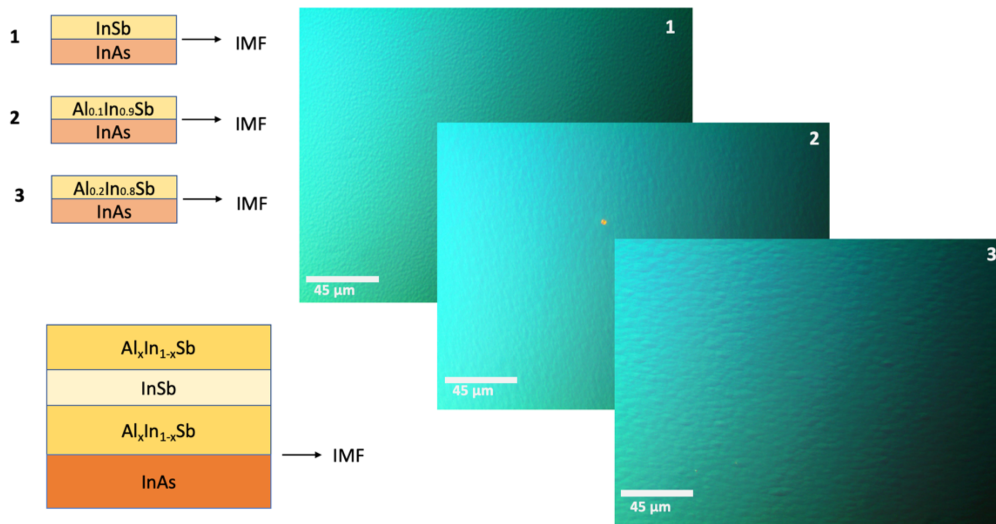

Fig.3. Nomarsky micrographs of (Al)InSb on InAs. The growth of InSb directly on InP has some orange-peel, this gets a bit more pronounced with the addition of Aluminum.

The surface morphology for all the layers is excellent, with some visible orange peel observed in the higher Al content samples. This can be seen in figure 3.

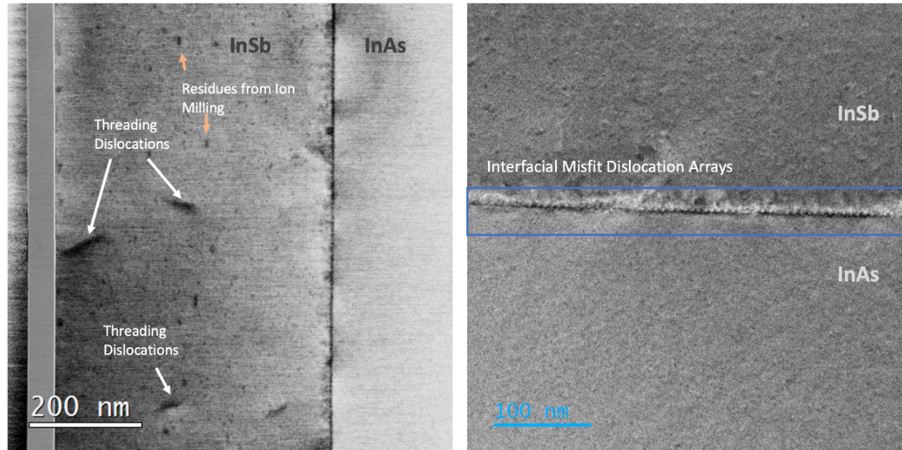

Fig. 4. Cross section TEM analysis of the inSb on InAs is shown. (Left) We can observe some residual threading dislocations in the sample indicating a density of $10^8/cm^2$. (Right) we see a clear formation of the IMF layer in the sample. This is the first confirmed growth of InSb on InAs using the IMF growth mode.

After the confirmation of the relaxation of the epilayers, the samples are investigated with a TEM and misfit dislocation array formations at the AlInSb/InAs interface are observed. The InSb/InAs growth clearly shows the presence of an IMF interface. This is the first instance where a high quality IMF growth is realized in a growth system other than GaSb on GaAs.

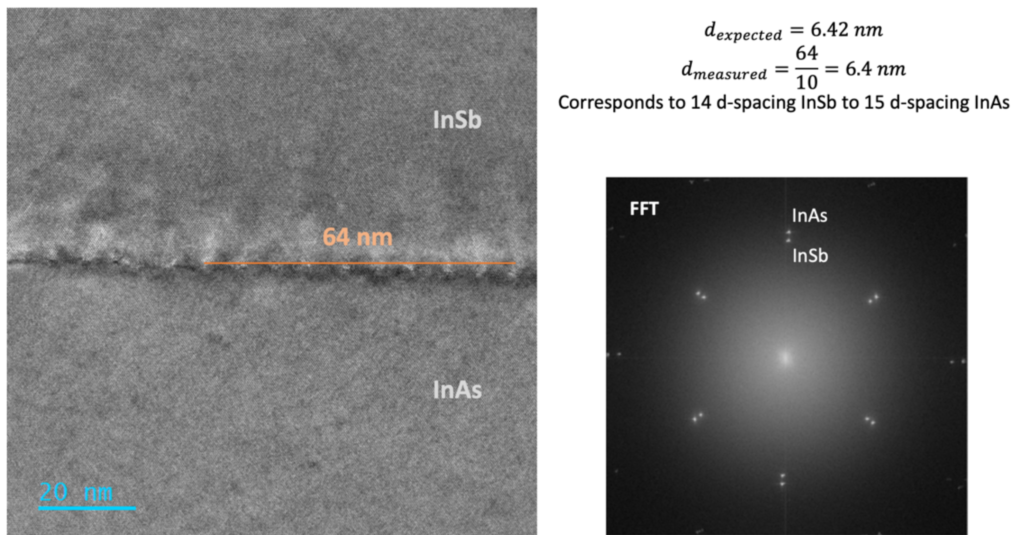

Fig. 5. Confirmation of the IMF growth mode using a direct distance measurement using X-TEM (Left) and using FFT analysis of the image (Right).

To determine the material quality, InSb quantum well grown with different Al concentration $Al_xIn_{1-x}Sb$ cladding layer is investigated by photoluminescence (PL) setup. We will present the comparison of detailed X-ray analysis of the buffer layers as well as TEM images to look at the

threading dislocation density of the materials. The comprehensive analysis of the InSb quantum well samples investigation with PL and TRPL results is shown below. See figure 5.

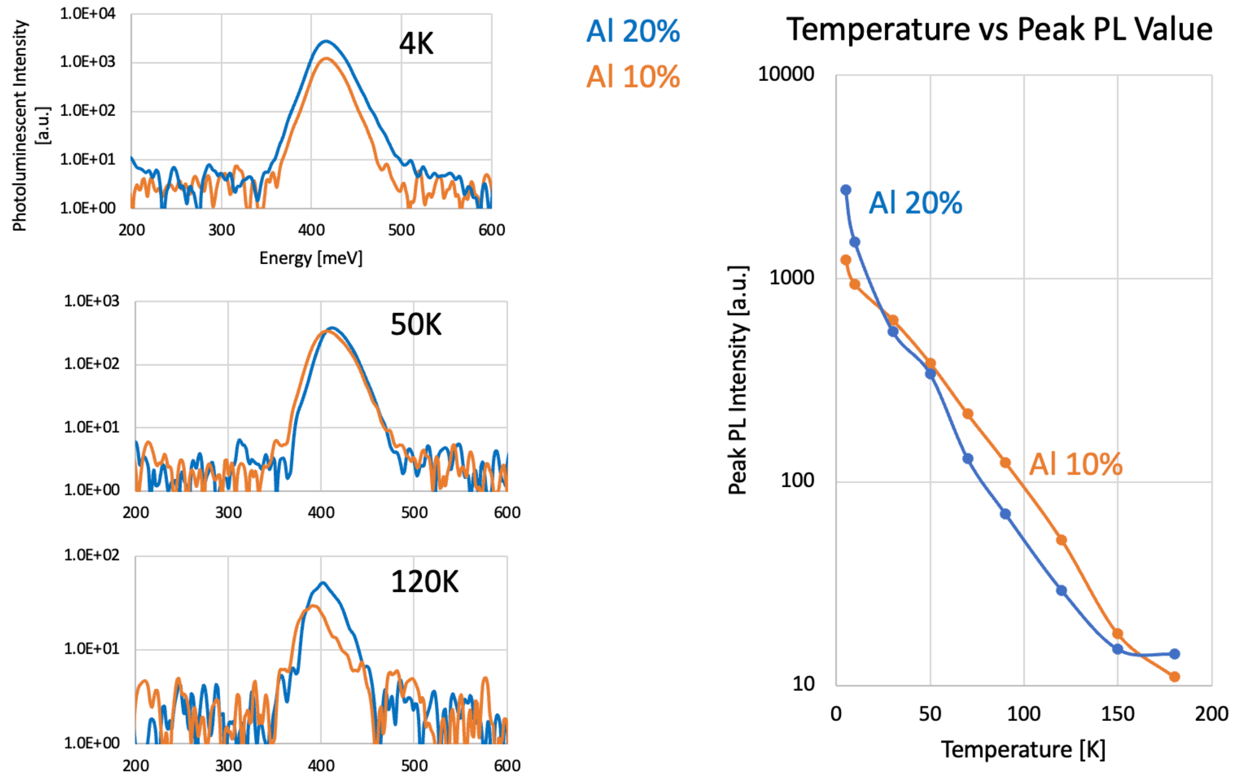

Fig. 5. Low temperature and Time resolved PL from InSb quantum wells grown on InAs.

1.B. IMF formation in growth of $In_{0.53}Ga_{0.47}Sb$ on InP

We present the growth of $In_{0.53}Ga_{0.47}Sb$ on InP using the interfacial misfit dislocation growth mode. The growth is performed by using an intermediate InGaAs layer and achieving an As for Sb anion exchange. Characterization results show the formation of an interfacial misfit dislocation array, however the epilayer shows significant phase segregation.

Narrow bandgap antimonide-based alloys such as $InAs_xSb_{1-x}$ can result in MWIR and LWIR detectors which are used for atmospheric remote sensing and medical devices. The ability to access lattice constants of ~ 6.3 Å could lead to significant breakthroughs for such devices. However, the lack of substrates between GaSb and InSb limits the composition options to realize fully relaxed $InAs_xSb_{1-x}$ epi-layers with high antimony percentage. In the past, it has been shown that interfacial misfit dislocation (IMF) array-based growth mode can be used to achieve instantaneous relaxation of antimonide layers with direct growth of GaSb on GaAs resulting in a dislocation density of ~ 10^8 dislocations/cm^2 and with a defect filter layer this value can be reduced to 10^7 dislocations/cm^2. In this period of performance, we demonstrate use of IMF-based growth to achieve direct growth of $In_{0.53}Ga_{0.47}Sb$ on InP substrate by using $In_{0.53}Ga_{0.47}As$ as an intermediate layer. The technique used involves the replacement of As with Sb under highly controlled temperature and III-V ratios. Thus, similar to GaSb/GaAs, it is our objective in this presentation to realize high-quality $In_{0.53}Ga_{0.47}Sb$ directly on $In_{0.53}Ga_{0.47}As$/InP.

(a) (b) (c)

Fig.6. TEM analysis of IMF formation between the GaSb/GaAs layers. Figure (a) shows all three layers, (b) is an SAED analysis of figure (a). (c) shows the growth interface between InGaAs on InP.

The alloys are grown using an elemental source Veeco ® Gen 10 molecular beam epitaxy (MBE) reactor with valved crackers for the Sb and As sources. The native oxide formed on the InP substrate is removed thermally at 540°C under arsenic overpressure. This process is followed by the growth of a 500 nm thick $In_{0.53}Ga_{0.47}As$ lattice-matched layer at a growth rate of 0.5 ML/sec. The $In_{0.53}Ga_{0.47}Sb$ layer is then grown by replacing antimony with arsenic. This is realized by first desorbing excess arsenic from the InGaAs layer by closing the Arsenic supply while the wafer is kept at growth temperature, for a duration of 30 seconds. At the end of this arsenic desorption step, Sb_2 is introduced without changing other parameters, thus allowing for the creation of a thin $In_{0.53}Ga_{0.47}Sb$ layer.

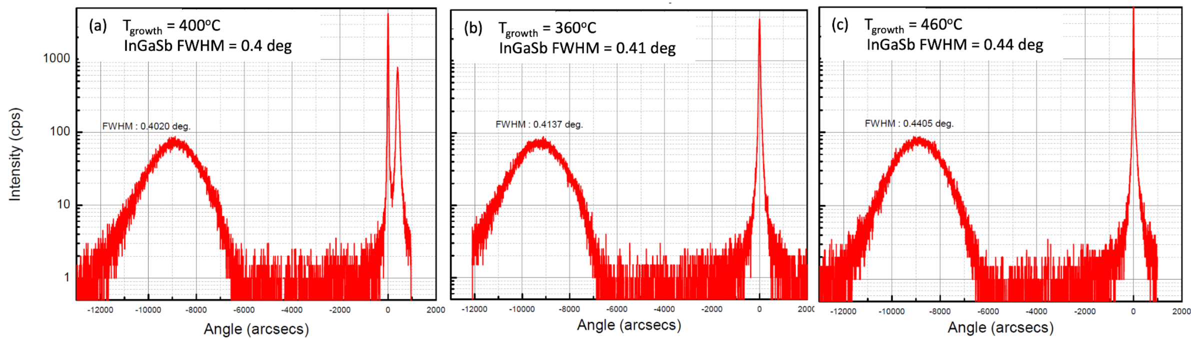

Fig.7: HR-XRD analysis of InGaSb IMF layers grown at 400, 360 and 460 degrees celsius. There is some change in FWHM of the InGaSb peak but the peaks are broad and symmetric.

We present the analysis of such samples with the InGaSb grown at a variety of growth temperatures. The baseline structure was grown at 400°C followed by two subsequent growths at 360°C and 460°C. Surface morphology, cross-section TEM, HR-XRD, and photoluminescence studies were conducted on these samples. The XRD analysis shows that the $In_{0.53}Ga_{0.47}Sb$ layer is fully relaxed, however the FWHM of the epilayer peak is extremely broad at ~ 1500 arcseconds. TEM analysis in most of the samples shows the presence of a periodic misfit dislocation array. However, at higher (atomic-resolution) images, there appear to be several different crystal

orientations present in the same image. In combination with the XRD data, we believe this indicates the possibility of compositional segregation in the InGaSb layer driven by miscibility gap issues.

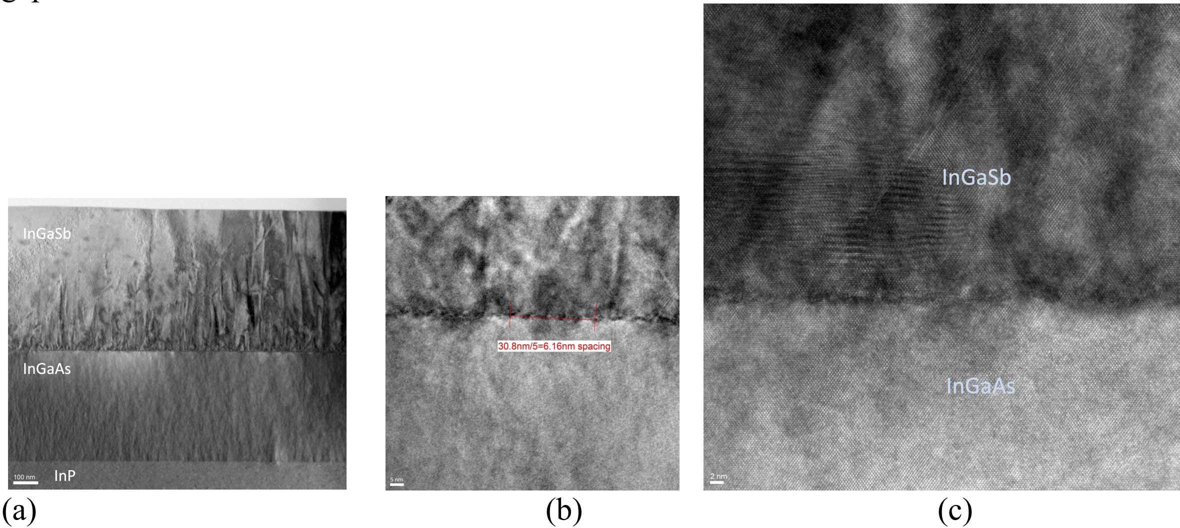

(a) (b) (c)

Fig.8: TEM analysis of the sample grown at 400 C shows the presence of an IMF layer between the InGaSb/InGaAs layers. Figure (a) shows all three layers, (b) shows the interface between InGaSb and InGaAs and the presence of a periodic misfit dislocation array and figure (c) is a high resolution image showing the presence of different crystal orientations in the growth .

Goal 2: Atomic-resolution structure imaging of interfacial defects in IMF growth mode.

The core structure of interfacial defects in a GaSb/GaAs(001) heterostructure have been determined using atomic-resolution structure imaging. Several different defect types, including Lomer edge dislocations, perfect 60° dislocations and dissociated 60° dislocations, were identified using Burgers circuit analysis. The majority (83%) of the eighteen analyzed interfacial defects were perfect 90° Lomer dislocations, with an average separation of 6.0$\pm$0.5nm. These defects had three different types of core structure: the well-known 5-7 ring shuffle-set, which were most commonly observed, as well as the 6-8 ring left-displaced glide-set and the 6-8 ring right-displaced glide-set. However, no symmetric glide-set Lomer dislocations were seen. The presence of single atomic columns at the core of the perfect 60° dislocation, and at the core of the 30° Shockley partial of the dissociated 60° dislocation, indicated that both of these defects belonged to the glide set.

High-resolution transmission electron microscopy (TEM)offers the attraction of being able to image dislocation cores with very high spatial resolution, and the technique has been widely used for many years to reveal the atomic structure of dislocation cores in semiconductor heterostructures. The recent generations of aberration-corrected electron microscopes (ACEMs) have the capability to routinely produce images with sub-angstrom level resolution, which enables direct atomic-structure imaging of dislocation cores in many semiconductors. This paper concentrates on atomic-scale characterization of interfacial defects occurring in an isovalent GaSb/GaAs(001) heterostructure, using aberration-corrected scanning TEM.

The GaSb/GaAs sample was prepared by molecular beam epitaxy (MBE) Cross-section TEM samples were prepared using mechanical polishing, dimpling and argon ion milling, with the

sample held at liquid-nitrogen temperature to minimize any irradiation-induced artefacts. Conventional TEM images were obtained using a JEOL 2010F microscope operated at 200 kV. Atomic-resolution STEM imaging was carried out using a JEOL ARM-200F microscope also operated at 200 kV. The probe convergence angle was 22 mrad, and the inner and outer collection angles for high-angle annular-dark-field (HAADF)-STEM imaging were 90 and 150 mrad, respectively.

Figure 9(a) shows a bright-field TEM micrograph of the GaSb/GaAs(001) heterostructure. A high density of threading defects and stacking faults is visible in the GaSb layer. As expected, the GaSb/GaAs interface also exhibits a high density of defects. Aberration-corrected STEM imaging was used to examine the atomic structure of the interfacial defects, and Fig. 9(b) shows a typical atomic-resolution HAADF-STEM image of the GaSb/GaAs interface region. Several different types of interfacial defects can be identified, including 60° and Lomer dislocations, as well as a short {111}-type intrinsic stacking fault propagating upwards from the plane of the interface.

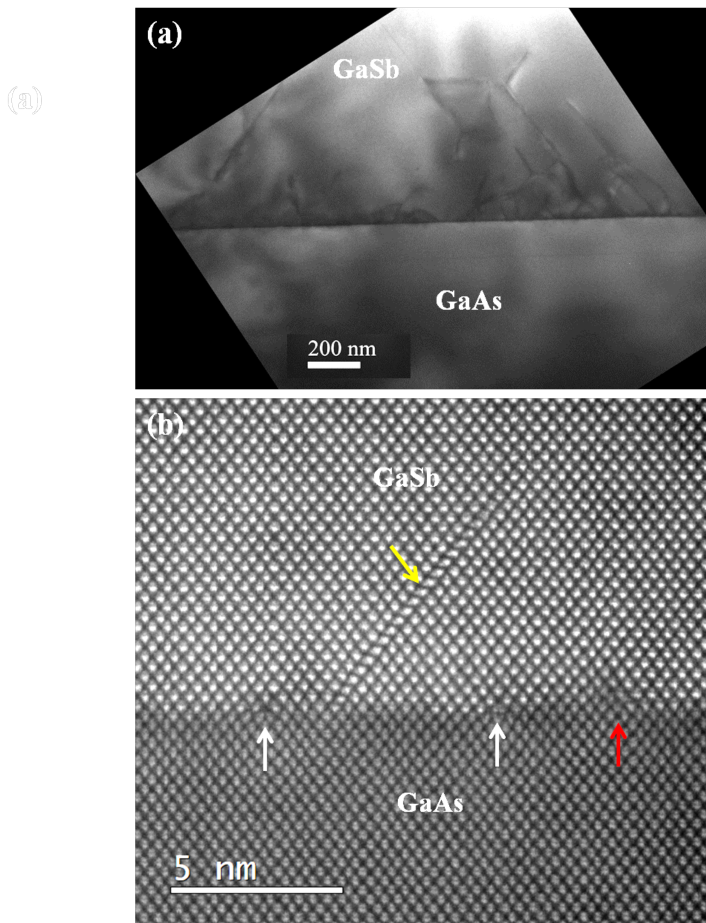

Fig. 9. (a) TEM micrograph of GaSb/GaAs(001) heterostructure revealing the crystalline quality and defect structure of the GaSb layer. (b) Atomic-resolution HAADF-STEM structural image of GaSb/GaAs heterointerface region showing short {111}-type intrinsic stacking fault (yellow arrow), 60° dislocation (red arrow) and two Lomer dislocations (white arrows).

Figure 10(a) shows a large-angle bright-field (LABF) STEM image of an interfacial defect at the GaSb/GaAs interface. The Burgers vector of the defect is determined by drawing a RH/FS (right-

hand/finish-start) Burgers circuit, and the arrow joining the finishing and starting points of the circuit indicates the Burgers vector. Thus, the Burgers vector here is identified to be $a/2[\bar{1}\bar{1}0]$, according to the directions shown on the figure, which constitutes a full lateral lattice translation. This perfect 90° dislocation is identified as a Lomer edge dislocation, since the $[1\bar{1}0]$ dislocation line direction, which is also the beam projection direction, makes a 90° angle with the $[\bar{1}\bar{1}0]$ Burgers vector direction. The atomic arrangements at the dislocation core can be directly determined based on the atomic-column intensities in the HAADF-STEM image of the same defect, as illustrated in Fig. 10(b). As represented by the schematic, the dislocation core consists of five-membered and seven-membered rings of atoms. This atomic arrangement corresponds to the shuffle-set variant of the two types of core structures of edge dislocations in diamond-cubic crystals, as originally proposed by Hornstra and also previously reported for the GaSb/GaAs interface by Wang *et al*.

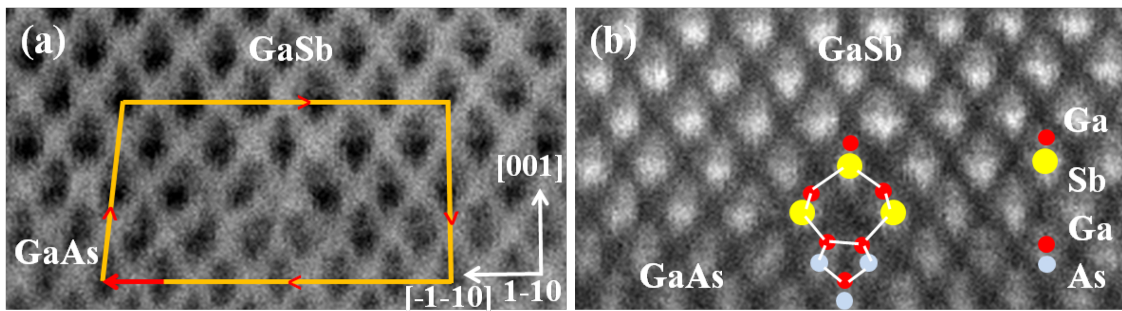

Fig. 10 (a) Atomic-resolution LABF-STEM structural image of interfacial dislocation at GaSb/GaAs interface, together with corresponding RH/FS Burgers circuit. (b) HAADF-STEM image of the same defect with structural model overlaid on the dislocation depicting the five-membered and seven-membered atomic ring arrangements at the defect core.

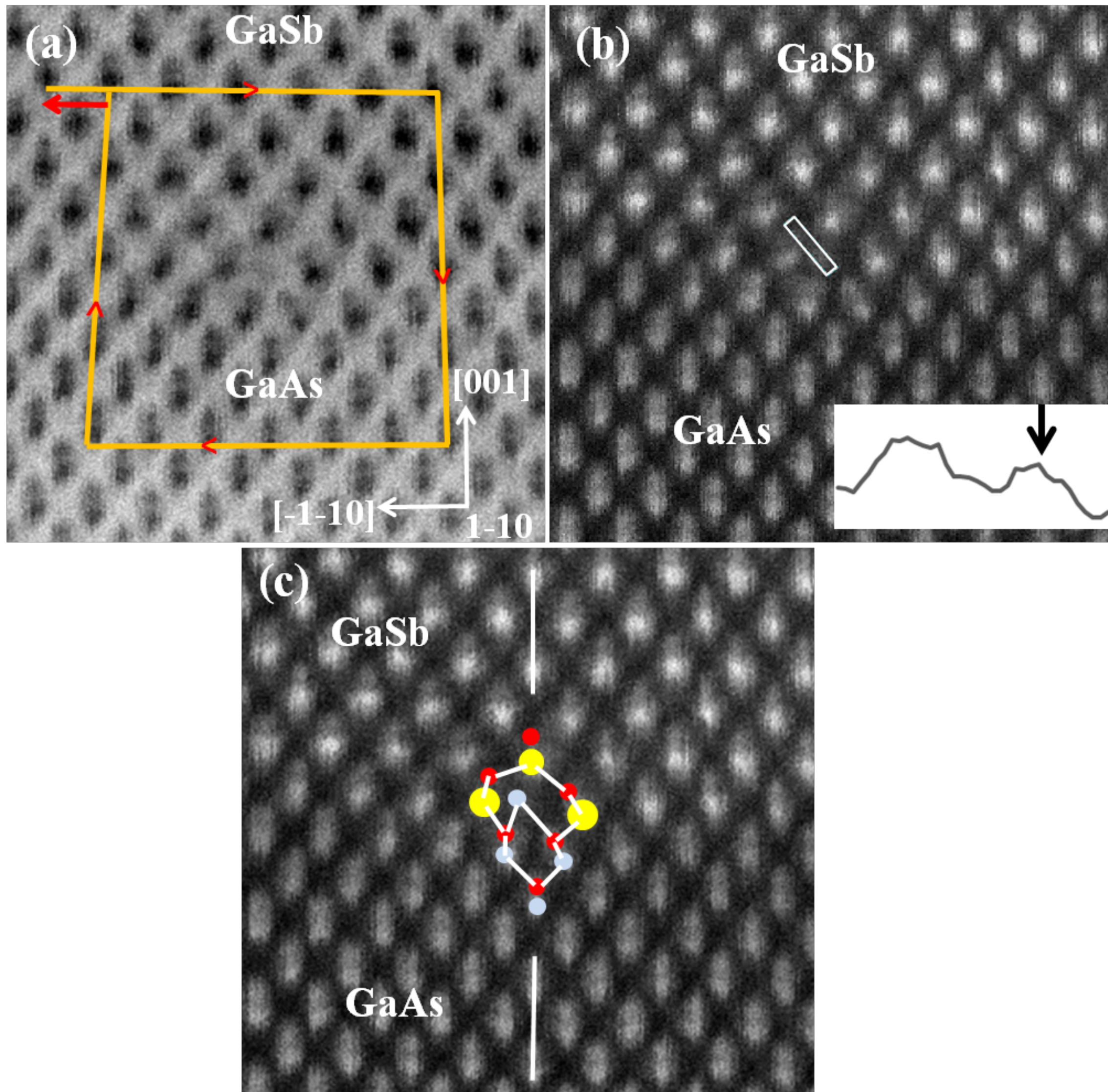

Fig. 11 (a) Atomic-resolution LABF-STEM image of dislocation located at GaSb/GaAs interface with corresponding RH/FS Burgers circuit. (b) HAADF-STEM image of the dislocation core and intensity profile (inset) revealing two distinct peaks corresponding to separate atomic columns. (c) Proposed atomic arrangement at dislocation core overlaid on HAADF-STEM image.

Figure 11(a) shows an atomic-resolution LABF-STEM image of another defect located at the GaSb/GaAs interface. A RH/FS Burgers circuit was drawn encompassing the defect in order to identify the Burgers vector, which was again determined to be $a/2[\bar{1}\bar{1}0]$, corresponding to a Lomer dislocation. Figure 11(b) includes an intensity profile across the HAADF STEM image of the same defect. This profile confirms the existence of a single atomic column at the core, which is displaced slightly towards the left-hand side with respect to the {220} median plane (marked by solid white vertical lines in Fig. 11(c)). Figure 11(c) depicts schematically the atomic arrangements at the dislocation core, which consist in this case of six-membered and eight-membered rings of atoms. This atomic configuration corresponds to the glide-set variation of a Lomer dislocation, as originally proposed by Hornstra and is formally identified as a left-displaced glide-set Lomer dislocation.

Figure 12(a) shows an aberration-corrected LABF-STEM structure image of yet another defect located at the GaSb/GaAs(001) interface, associated in this case with an interface step. A RH/FS Burgers circuit drawn around the dislocation again identifies the Burgers vector as $a/2[\bar{1}\bar{1}0]$. This Burgers vector is equivalent to a full lattice translation with a 90° angle with the $[1\bar{1}0]$ dislocation line direction, and thus the defect is confirmed to be a Lomer edge dislocation. Figure 12(b) includes an intensity profile that indicates the presence of an atomic column at the core (marked by the arrow), albeit displaced slightly towards the right with respect to the {220} median plane (marked by the solid white lines in Fig. 4(c)). The atomic arrangement of the dislocation core, based on the contrast of the HAADF-STEM image, is shown schematically in Fig. 4(c). The dislocation core consists of six-membered and eight-membered rings of atoms. Careful observation of the intensity profile across the interface indicates that the dislocation is associated with an interfacial atomic step, as shown in Fig. 4(c). Thus, this specific dislocation is identified as a right-displaced glide-set Lomer dislocation that incorporates an atomic step on one side of the defect.

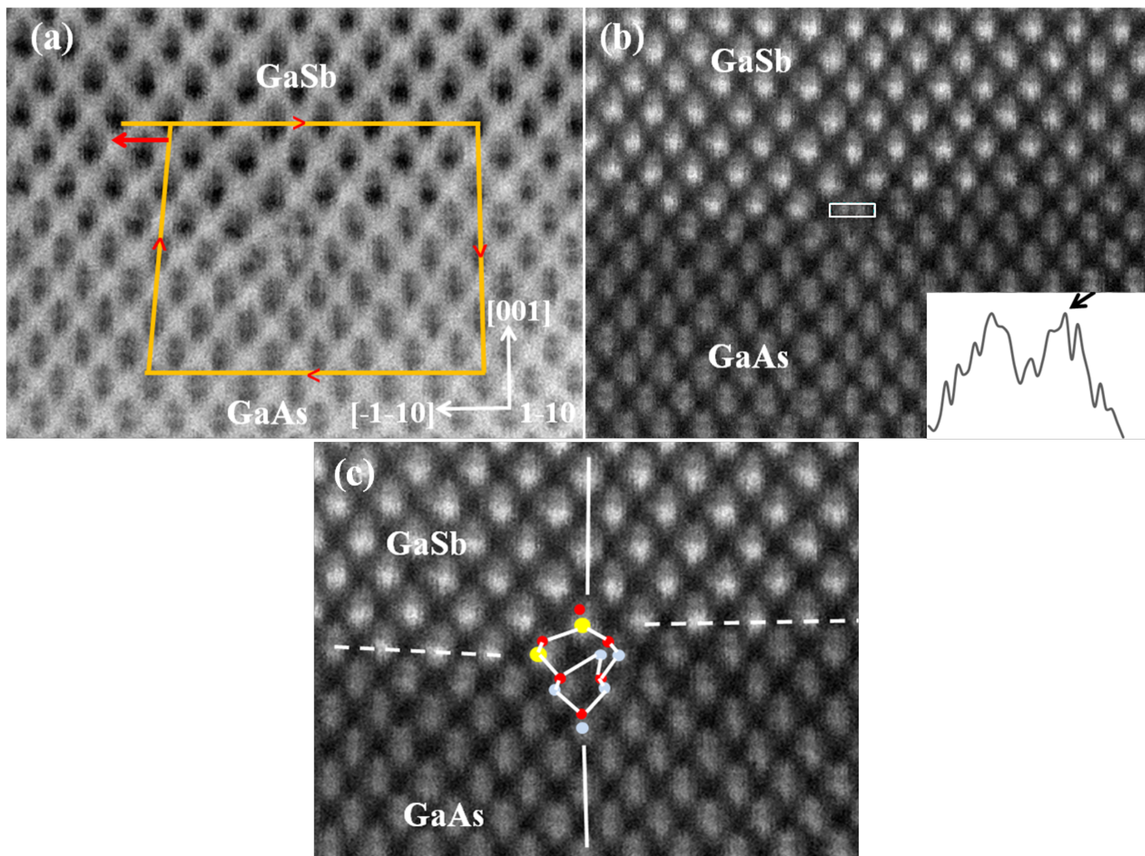

Fig. 12. (a) Aberration-corrected LABF-STEM image of interfacial dislocation at GaSb/GaAs interface with corresponding RH/FS Burgers circuit. (b) HAADF-STEM image and intensity profile from HAADF-STEM image of dislocation core revealing two distinct peaks (the one corresponding to the atom centrally located in the defect core is marked by arrow in the inset). (c) Proposed atomic arrangement of defect core overlaid on HAADF-STEM image. Dotted line shows location of GaSb/GaAs interface.

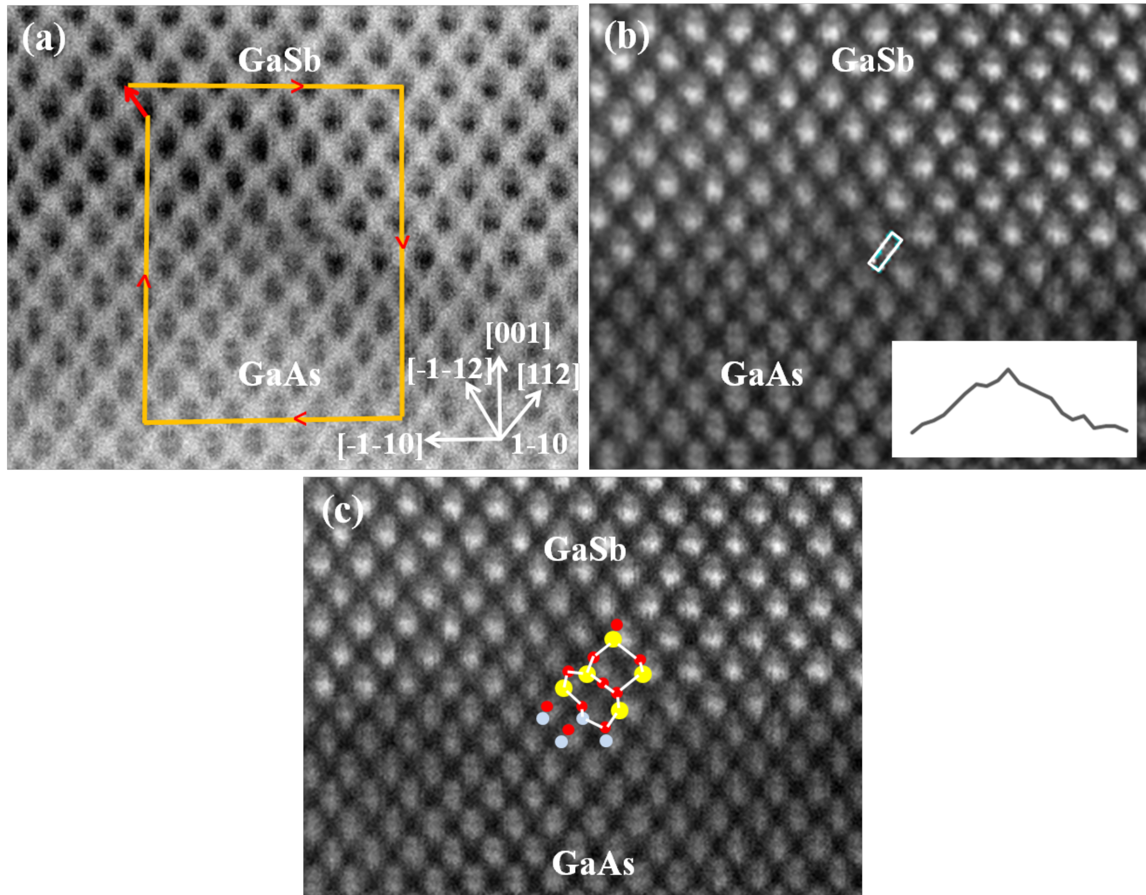

Fig. 13. (a) Aberration-corrected LABF-STEM structure image of interfacial defect in the GaSb/GaAs heterostructure with corresponding RH/FS Burgers circuit. (b) HAADF-STEM image and intensity profile obtained from HAADF-STEM image reveal single atomic peak at defect core. (c) Proposed atomic arrangement of defect core overlaid on HAADF-STEM image.

Figure 13(a) shows an atomic-resolution LABF-STEM image of a fourth type of GaSb/GaAs interfacial defect, together with the corresponding RH/FS Burgers circuit. The closure vector here is identified as $a/4\ [\bar{1}\bar{1}2]$, according to the directions shown on Fig. 13(a). This arrangement would correspond to the projected component of a 60° dislocation with a Burgers vector of either $a/2[\bar{1}01]$ or $a/2[0\bar{1}1]$, which lies in a (111) slip plane. Figure 13(b) includes an intensity profile from the HAADF-STEM image of the dislocation core, which confirms the presence of a single atomic column at the defect core. Figure 13(c) shows a model of the dislocation core overlaid on the HAADF-STEM image showing the most probable atomic arrangement. The presence of the single As atomic column at the core confirms that the dislocation belongs primarily to the glide-set [12].

Figure 14 shows an atomic-resolution HAADF-STEM image of a stacking fault originating at the GaSb/GaAs(001) interface, and extending upwards into the GaSb layer. A RH/FS Burgers circuit was drawn to encompass the partial dislocations at both ends of the dissociated defect, and the closure vector here is identified as $a/4\ [\bar{1}\bar{1}2]$. This would correspond to the projected component of either $a/2[0\bar{1}\bar{1}]$ or $a/2[\bar{1}0\bar{1}]$ Burgers vectors of an undissociated 60° dislocation that lies in a $(\bar{1}\bar{1}1)$ slip plane. Thus, this 60° dislocation has dissociated into 30° Shockley partial

and 90° Shockley partial dislocations, as observed previously for the GaAsSb/GaAs(001) heterostructures.[13] The dissociation reaction can be written as:

$a/2[0\bar{1}\bar{1}]$ = $a/6[1\bar{2}\bar{1}]$ + $a/6[\bar{1}1\bar{2}]$

OR

$a/2[\bar{1}0\bar{1}]$ = $a/6[\bar{2}1\bar{1}]$ + $a/6[\bar{1}\bar{1}\bar{2}]$

60° perfect   30° partial 90° partial

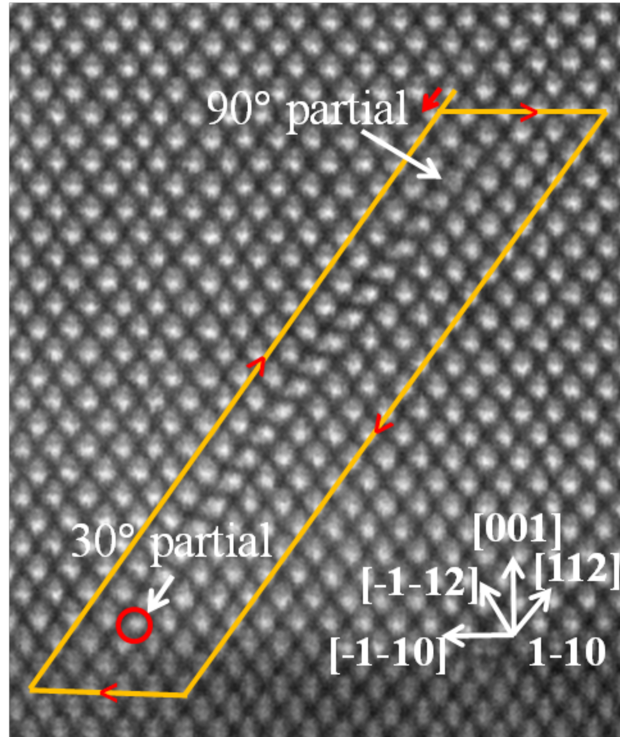

Fig. 14. Aberration-corrected HAADF-STEM image of dissociated 60° dislocation at the GaSb/GaAs(001) interface and corresponding RH/FS Burgers circuit.

The 30° partial is the leading partial dislocation and is located right at the compressively-strained GaSb/GaAs interface. The core of the 30° Shockley partial dislocation contains the characteristic single atomic column, identified here as corresponding to Sb, indicating that the dislocation belongs to glide-set. The corresponding 90° Shockley partial dislocation, which is the associated trailing partial dislocation, is located in the GaSb layer.

Once the different types of defects and the atomic arrangements of their core had been identified, their relative frequency of occurrence at the interface was determined. Out of the eighteen defects analyzed, twelve were classic 5-7 ring shuffle-set Lomer dislocations, two defects were left-displaced 6-8 ring glide-set Lomer dislocations, one was right-displaced 6-8 ring glide-set Lomer dislocation, two were perfect 60° dislocations and one was a dissociated 60° dislocation. The average distance between the Lomer dislocations at the interface was measured to be 6.0 ± 0.5 nm. However, the Lomer dislocations were not regularly spaced along the interface, most likely because of the occurence of the different defect types as well as the presence of occasional interface steps. Only a relative few were associated with these monolayer steps, indicating that the presence of an interface step was not a prerequisite for formation of a Lomer dislocation.

Goal 3: Mid-Infrared Interband Cascade Light Emitting Devices Grown on off-axis Silicon Substrates

We report the growth of GaSb-based mid-infrared interband cascade light emitting devices (ICLEDs) on 4 degree offcut silicon substrates with 12% lattice mismatch. Four wafers produced functioning devices, with variations from wafer to wafer but relatively uniform performance of devices processed from a given wafer. The full width at half maxima for the (004) GaSb rocking curves were as narrow as ~ 163 arc seconds, and the root mean square surface roughness as small as 3.2 nm. For comparison, a control structure was also grown to the same design on a GaSb substrate. Devices were fabricated from all 5 wafers and mounted epitaxial-side-up to evaluate their electro-optical properties. The control devices had good material and spectral emission properties, and low leakage currents that indicated favorable material processing. However, the emission efficiencies and series resistances of the control devices were severely reduced by heating at modest continuous wave (cw) currents due to a high thermal resistance for heat dissipation via the GaSb substrate. By contrast, the same reductions were not observed for devices grown on silicon because of its much higher thermal conductivity. As compared to our previous best-performing standard ICLEDs grown on GaSb, which were mounted epitaxial-side-down and had anti-reflection (AR) coatings on the substrate output surfaces, all of the devices on silicon had higher leakage currents and higher series resistances. However, taking into account the differences in device architecture the efficiencies at high cw currents for the best devices on silicon were approximately 75% of those for the previous standard. At an injection current of 100 mA, the best 200 μm-diameter mesas with 22 active stages, no AR coating, and a top contact that blocks 25% of the output produced 184 μW of cw output power when operated at T = 25 °C, and 140 μW at 85 °C. Possible factors governing whether a given growth on silicon will produce high-performance ICLEDs are discussed, although no definite conclusions are possible at this time.

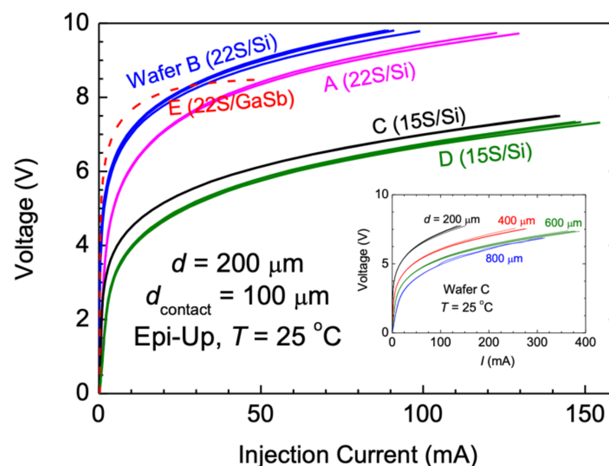

Fig. 15. Cw I-V characteristics at room temperature for ICLEDs with 200 μm diameters processed from Wafers A-D grown on offcut silicon, as well as a device from the control Wafer E. The inset shows J-V characteristics for multiple devices with all four mesa diameters processed from Wafer C.

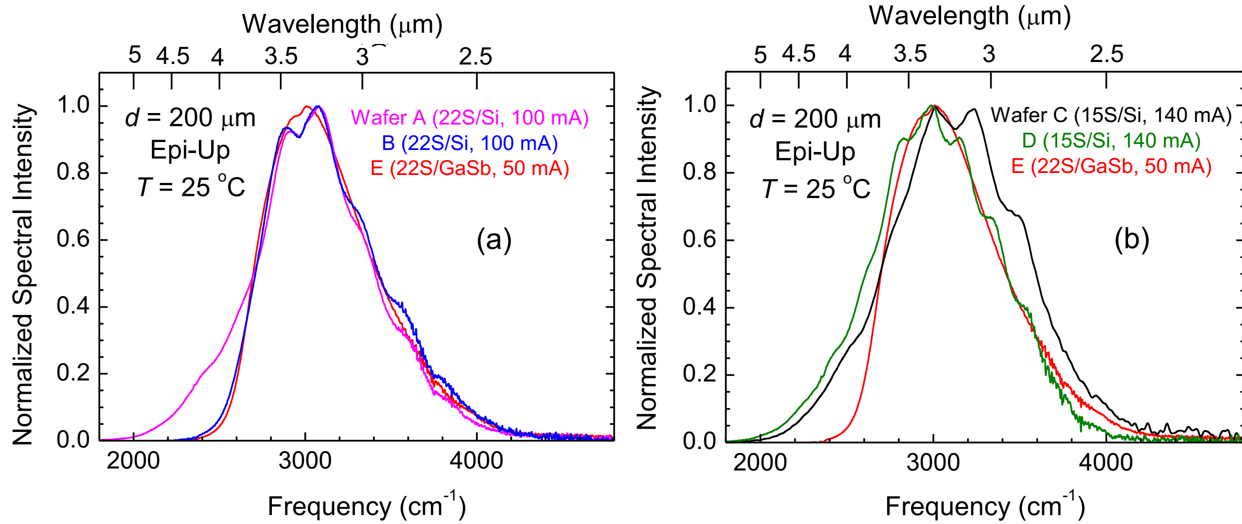

Fig. 16. Normalized cw emission spectra at T =25 ℃ from representative ICLEDs with 200 µm diameters processed from offcut silicon Wafers (a) A and B (22 stages) at current 100 mA and (b) C and D (15 stages) at current 140 mA. Both plots include the spectrum for a device processed from the control Wafer E grown on GaSb at current 50 mA. The undulations in the spectra for devices grown on Si are Fabry-Perot fringes.

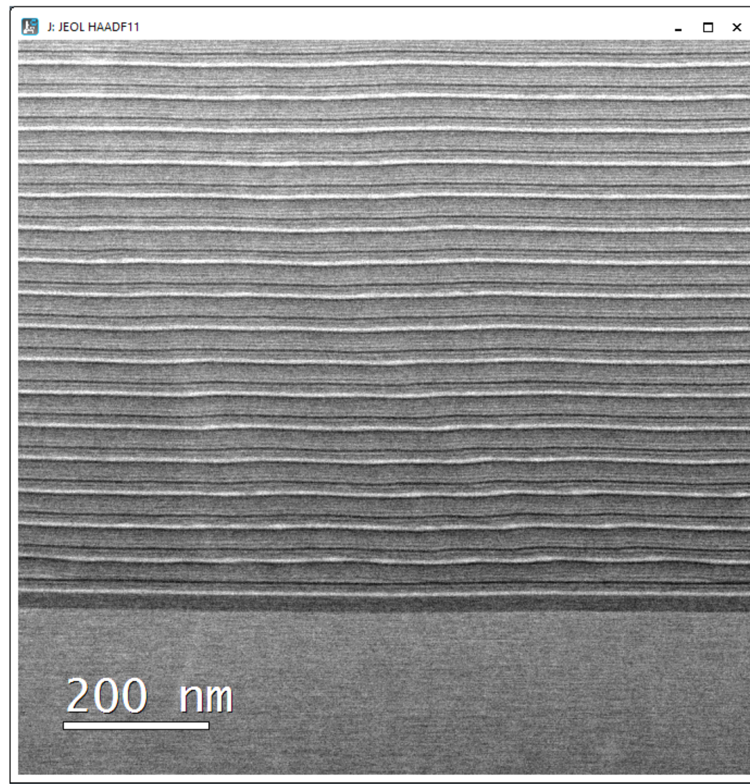

Fig. 17. Very low defect density ICLEDs grown on Antimonide buffers on Silicon. The buffers were developed in this project and the ICLED designs were developed at NRL.